Forest Ecology and Management 585 (2025) 122709

Contents lists available at ScienceDirect

Forest Ecology and Management

journal homepage: www.elsevier.com/locate/foreco

A linkage between fire temperature and satellite-derived fire severity index in a north-central appalachia mixed-oak forest

Ziyu Dong, Roger A. Williams *

School of Environment and Natural Resources, The Ohio State University, Columbus, OH 43210, USA

ARTICLE INFO

Keywords:
Fire temperature
Fire severity
DNBR
Topography
Seasonality

ABSTRACT

The Differenced Normalized Burn Ratio (dNBR) is a widely used satellite-based index in fire severity assessment. However, gaps remain in the linkage between dNBR and fire temperature. This study aims to investigate the relationship between dNBR and fire temperature, demonstrating the potential of dNBR to retrospectively infer fire temperatures and generate spatially continuous fire temperature maps, which are challenging to achieve through fieldwork. A total of 209 plots were established in Zaleski State Forest, southeast Ohio. Three prescribed fires were conducted during spring and fall. The recorded fire temperatures were analyzed with both Landsat 8–9 and Sentinel 2-derived dNBR. Seasonal and spatial patterns of fire severity were also examined. The results indicate that both Landsat 8–9 and Sentinel-2 derived dNBR displayed significant positive relationships with fire temperature ($R^2 = 0.378$–0.509) for the spring burns, with Sentinel 2 fitting better than Landsat 8–9. No significant relationships were found in the fall burn between fire temperatures and dNBR for both sensors. The comparison between spring and fall burns revealed seasonal variation in satellite performance, with Sentinel 2 capturing higher dNBR values compared to Landsat 8–9 in the spring but Landsat 8–9 capturing higher dNBR values in the fall. These findings suggest a potential method to create spatial continuous fire temperature maps by retrospectively inferring fire temperature using satellite-based dNBR, filling the gaps that fieldwork can only measure discrete fire temperature.

1. Introduction

Effectively assessing and monitoring fire intensity and severity are critical components of fire management (Agbeshie et al., 2022). These factors have been widely studied due to their importance in understanding post-fire ecological responses, including tree mortality, organic material consumption, and vegetation succession (Bataineh et al., 2022; Perry et al., 2011). Although both fire intensity and fire severity are essential concepts in fire science, they represent distinct phenomena. Specifically, fire severity describes the effects of fire on ecosystems, focusing on fire-induced changes in vegetation and soils (Keeley, 2009). Fire intensity, in contrast, is more focused on fire behavior itself which represents the amount of heat released during the combustion process (Keeley, 2009). Based on the distinct differences between fire severity and fire intensity, a long-standing question for fire researchers is to understand the relationships between fire severity and fire intensity, and subsequently explore whether fire severity patterns can be utilized to infer fire intensity retrospectively (Gale et al., 2021; Hammill and Bradstock, 2006).

Current methods for measuring fire intensity continue to be limited and there is a lack of an instrument that can measure fire intensity directly because fire intensity represents the energy released during various phases of a fire (Silvani and Morandini, 2009). Alternative metrics such as fire temperature, residence time, and heat fluxes are usually used as surrogates for different research purposes (Keeley, 2009). As an alternative metric, fire temperature has a long history in the study of fire science and it can be used to estimate the flame rate of spread and fire contour in the context of fire modeling (Wardihani et al., 2018). However, the restriction of ground fire temperature measurements is that the measurements are discrete field-scale point measurements (Mueller et al., 2018). For example, Molina et al., (2022) used thermocouples at each spot mark to measure fire temperature and calculate fire rate of spread. Iverson et al., (2004) applied both thermocouples and temperature paints to monitor spatial and temporal patterns of prescribed fires by putting them into each study plot, with neither of them providing a spatial continuous fire temperature map.

In addition, fire radiation power (FRP) is also is a key factor in estimating fire temperature and assessing fire intensity owing to its

* Corresponding author.
E-mail address: williams.1577@osu.edu (R.A. Williams).

https://doi.org/10.1016/j.foreco.2025.122709
Received 24 February 2025; Received in revised form 1 April 2025; Accepted 2 April 2025
Available online 6 April 2025

relation to the rates of combustion, energy released from the flaming and smouldering, and biomass consumption (Freeborn et al., 2008; Kremens et al., 2012; Wooster et al., 2005). The use of long-wave infrared imagery is a common approach to infer fire radiative power and provide spatial continuous temperature maps. This approach has been applied across various remote sensing platforms, such as ground-based platforms, airborne platforms, and satellite sensors (Dickinson et al., 2016; Hudak et al., 2016; Kaufman et al., 1998). The method of using hyperspectral data to retrieve active fire temperature by fire modeling has also been assessed by Dennison et al., (2006). With advancements in technology, Unmanned Aerial Vehicles (UAVs) equipped with thermal, RGB, or visible (VIS) cameras have been increasingly utilized to provide real-time fire information during controlled burns (Ambrosia et al., 2003; Aragon et al., 2020; Kanand et al., 2020). Nonetheless, even though the long-wave infrared imagery or UAVs mounted with multi-sensors can provide spatial continuous fire temperature maps, the cost and technology requirements limit their use (Akhloufi et al., 2021). Therefore, a more accessible and cost-efficient approach is needed to map fire temperature, such as using satellite images to detect vegetation damage (fire severity) and infer patterns of fire temperature.

Satellite-related remote sensing techniques enable efficient fire management planning in the relevance of assessing large-scale fire severity and post-fire restoration (Allison et al., 2016; Delcourt et al., 2021). It can provide spatial continuous maps for fire severity with different resolutions from various sensors (Quintano et al., 2018). The Normalized Burn Ratio (NBR) is one of the most commonly used satellite-derived metrics for mapping and quantifying fire severity (Roy et al., 2006). It is computed by near-infrared (NIR) and shortwave infrared (SWIR) bands from satellite imagery and is sensitive to the changes caused by fire, such as the amount of chlorophyll content in plants, moisture, char, and ash in the soil (Parks et al., 2014). The research regarding fire severity assessment combined with NBR index utilization has acquired increased attention ((Achour et al., 2022; Delcourt et al., 2021; Miller et al., 2009)). Previous studies examined the utilization of fire severity maps to detect fire refugia and unburnt patches within large wildfires, providing insight into applying remote sensing-derived fire severity maps to understand fire regimes or anticipate ecological responses (Cansler and McKenzie, 2014; Collins et al., 2019). However, a disconnect was found between remote sensing research and fire behavior knowledge (Gale et al., 2021), in which a linkage between fire severity and fire temperature is needed as fire temperature focuses more on fire behavior and provides more insights into post-fire fire behavior assessment.

To build a linkage between satellite-based metrics and fire temperature, this study explores the relationship between field-measured fire temperature and remote sensing-derived Differenced Normalized Burn Ratio (dNBR), providing a potential method to use spatial continuous fire severity values to infer fire temperature retrospectively. The objectives of this study were 1) to determine the relationship between remote sensing-derived dNBR with fire temperature, 2) to compare the performance of Landsat 8 and Sentinel-2 in capturing the relationship between fire severity and fire temperature, and 3) to explore the seasonal and spatial patterns of fire severity.

2. Materials and methods

2.1. Study site description

The study area was located within the Zaleski State Forest, southeast Ohio. Three study sites were previously selected to conduct prescribed burns in the fall or spring. The first site is Morgan Hollow (39.3593°N, 82.3102°W) encompassing an area of 144 acres, which was burned on March 21, 2022; the second site is Stony Creek (39.3464°N, 82.3384°W) encompassing an area of 224 acres, which was burned on November 11, 2023; and the third site is Loper Hollow East (39.3355°N, 82.3017°W) encompassing an area of 245 acres, which was burned on March 13, 2024 (Fig. 1).

2.2. Field measurements

A total of 209 circular 0.04 ha sample plots were established across the three study sites for the purpose of collecting multiple data, including forest attributes and fuel data, which were not specifically for this study. The plot locations were recorded by Garmin GPSMAP 64sx with an accuracy of 3 m. These plots were approximately 60 m apart from each other (depending on the accessibility and forest edge) and distributed evenly in a gridwork in each study site, with 93 plots in Morgan Hollow, 100 plots in Stony Creek, and 16 plots in Loper Hollow East.

Pyrometers were used to measure fire temperatures at each plot center and installed before each fire. The pyrometer consists of aluminum tags painted with temperature-sensitive paint (Tempilaq®) and attached to a metal pin that is inserted into the ground (Schwemlein and Williams, 2007). On each aluminum tag, temperature-sensitive paints will be applied, each with a different melting point (149°C, 177°C, 204°C, 260°C, 343°C, 371°C, 399°C, 427°C, 454°C, 482°C, 510°C, 538°C, 593°C, 649°C, and 704°C), as a means to record the maximum fire temperature (Boerner et al., 2000; Iverson et al., 2004; Schwemlein and Williams, 2007). Pyrometers were collected immediately after each burn.

HOBO dataloggers connected with K-type thermocouples were used to collect fire temperatures to correct and calibrate pyrometer readings. A total of 39 time series of temperature were recorded with K-type thermocouples, using the maximum temperature in each series to calibrate the maximum fire temperature measured by pyrometers. Specifically, 12 thermocouples were placed at Morgan Hollow, 11 thermocouples were placed at Stony Creek, and 16 thermocouples were placed at Loper Hollow East. The plots where thermocouples were located were selected randomly at each study site. Thermocouples were placed at the plot center on the day of the burn and collected immediately after the fire. The probe of each thermocouple was placed right on each pyrometer to reduce the error between the two measurements. The maximum temperature was recorded and compared over two measurements.

2.3. Fire temperature calibration

Since pyrometers can only provide estimated ranges of fire temperature, the pyrometer readings were calibrated by thermocouples. The linear regression between maximum pyrometer reading and maximum thermocouple reading was examined. All the pyrometer readings were calibrated based on the regression equation.

2.4. Imagery collection and processing

Pre- and post-fire Landsat 8–9 imagery processed to Level 1TP were downloaded from USGS (https://earthexplorer.usgs.gov/), in which Level 1TP represents Level-1 Terrain Precision corrected product, meaning the images that have undergone radiometric and geometric corrections. The Landsat 8–9 raw images were then pre-processed to correct the atmospheric discrepancies by ArcGIS pro-3.2.1. Sentinel-2 imagery processed to Level-2A was downloaded from the Sentinel Hub EO Browser (sentinel-hub.com) website. The Level-2A data means the images have been atmospherically corrected to provide surface reflectance. The closest cloudy-free images to the fire occurrence dates were downloaded (Table 1).

The NBR was computed using the NIR band and SWIR band as follows Eq. 1:

$$NBR = \frac{\mathrm{NIR} - SWIR}{\mathrm{NIR} + SWIR} \tag{1}$$

For Landsat 8–9, the 30-meter resolution of band 5 (near-infrared,

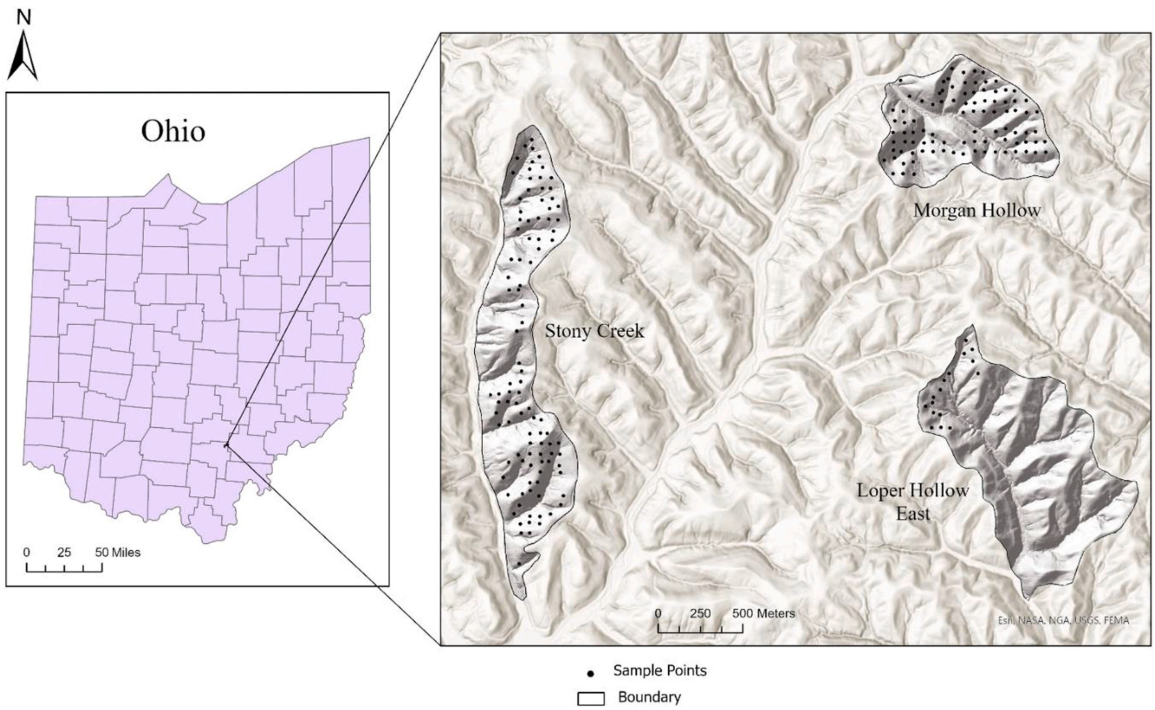

Fig. 1. Location of the study sites within the Zaleski State Forest, southeast Ohio.

Table 1
Summary of image acquisition for three fire locations.

Sites	Fire date	Area (acres)	Sources	Pre-fire image date	Post-fire image date	Bands	Spatial Resolution
Morgan Hollow	3/21/2023	144	Landsat 8–9 L1TP	3/20/2023	4/13/2023	Band 5, Band 7	30 m
			Sentinel 2 L2A	3/20/2023	4/09/2023	Band 8, Band 12	10 m
Stony Creek	11/6/2023	224	Landsat 8–9 L1TP	10/23/2023	11/08/2023	Band 5, Band 7	30 m
			Sentinel 2 L2A	11/05/2023	11/10/2023	Band 8, Band 12	10 m
Loper Hollow East	3/13/2024	245	Landsat 8–9 L1TP	2/20/2024	4/07/2024	Band 5, Band 7	30 m
			Sentinel 2 L2A	3/04/2024	3/24/2024	Band 8, Band 12	10 m

NIR) and band 7 (shortwave infrared, SWIR) was utilized. For Sentinel-2, the 10-meter resolution of band 8 (NIR) and band 12 (SWIR) was used. The dNBR was computed by taking the difference between the pre- and post-fire Normalized Burn Ratio (NBR), which is expressed as Eq. 2:

$$dNBR = \text{pre NBR} - post\ NBR \qquad (2)$$

2.5. Statistical analysis

All data analyses were performed using R statistical software version 4.3.3 (R Core Team, 2024). The linear regression model was created between maximum fire temperature measured by pyrometers and maximum fire temperature measured by K-type thermocouples. The linear regressions between dNBR and fire temperature, including both uncalibrated and calibrated maximum pyrometer readings, were conducted for Landsat 8–9 and Sentinel-2 imagery over spring and fall seasons. Two-way ANOVA followed by a standard Bonferroni correction and a post-hoc Tukey–Kramer test (significance level $\propto = 0.05$) was conducted to compare dNBR values among aspects (N, E, S, W) and seasons.

3. Results

3.1. Fire temperature calibration

The linear regression between maximum pyrometer reading and

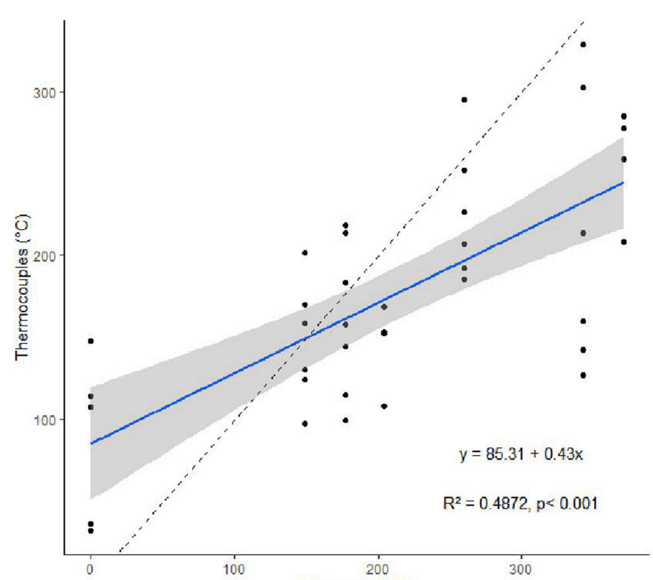

Fig. 2. The relationship between pyrometer-measured fire temperature (°C) and thermocouple-measured fire temperature (°C) (n = 39). The dashed black line represents the 1:1 line.

thermocouple reading was examined in the Fig. 2. The results showed that the maximum pyrometer reading displayed a positive correlation with thermocouple readings with an R^2 of 48.72 % ($p < 0.001$). All the pyrometer readings were calibrated based on the equation shown in Fig. 2.

3.2. Relationship between dNBR and fire temperature

To assess the utilization of dNBR for inferring fire temperature within the study area, simple linear regressions between fire temperature measured by pyrometers and fire severity index (dNBR) were conducted. Both Sentinel-2 and Landsat 8–9 derived dNBR displayed a significant positive correction with fire temperature in the spring (Fig. 3A). Specifically, the dNBR derived by Sentinel-2 displayed a higher correspondence to fire temperature with an R^2= 0.44 (n = 209, $p < 0.001$, Eq. 1) compared to dNBR derived by Landsat 8–9 with an R^2= 0.378 (n = 209, $p < 0.001$, Eq. 2). However, there were no significant correlations in the fall burn for both sensors ($p > 0.05$, Fig. 3B).

$$\text{Landsat8}-9: dNBR \times 10^3 = 23.43 + 0.3582 \times \text{Pyrometer} \tag{1}$$

$$\text{Sentinel2}: dNBR \times 10^3 = 63.56 + 0.4180 \times \text{Pyrometer} \tag{2}$$

Simple linear regression also examined the relationship between calibrated -pyrometer readings and dNBR derived by the two sensors (Fig. 3C–D). The results showed that the calibrated pyrometer readings displayed a significant positive relationship with Sentinel 2 and Landsat 8–9 derived dNBR for the spring burns, and the R^2 increased from the uncalibrated pyrometer readings for both sensors (Fig. 3C). The R^2 increased to 0.423 (n = 209, $p < 0.001$, Eq. 3) for the relationship between calibrated-pyrometer reading with dNBR derived by Landsat 8–9, and R^2 increased to 0.509 (n = 209, $p < 0.001$, Eq. 4) for the relationship between calibrated-pyrometer reading with dNBR derived by Sentinel 2. Consistent with the relationship between the original pyrometer, there was no significant correlation in the fall burn for both sensors ($p > 0.05$, Fig. 3D).

$$\text{Landsat8}-9: dNBR \times 10^3 = 10.18 + 0.4148 \times \text{Pyrometer} \tag{3}$$

$$\text{Sentinel2}: dNBR \times 10^3 = 46.85 + 0.4916 \times \text{Pyrometer} \tag{4}$$

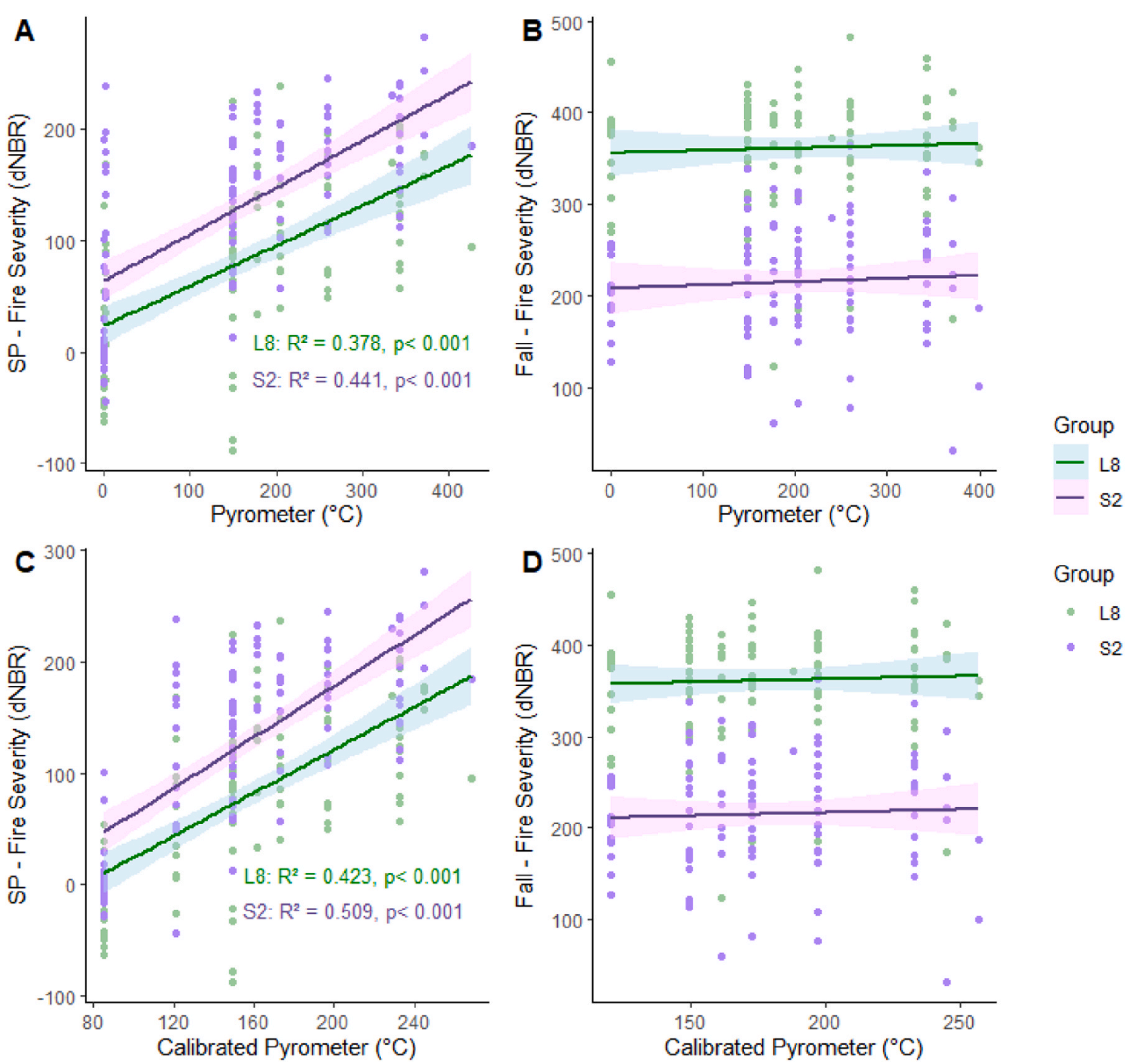

Fig. 3. The linear relationship between uncalibrated fire temperature and dNBR (scaled by 10^3) derived from Landsat 8–9 and Sentinel 2 over (A) spring and (B) fall burns (n = 209), and the linear relationship between calibrated-fire temperature and dNBR over (C) spring and (D) fall burns.

3.3. Comparison between the two sensors

Differenced Normalized Burn Ratio (dNBR) maps of the three study sites over two types of imagery are shown in Fig. 4. For the two spring burn sites, Morgan Hollow and Loper Hollow East, the Sentinel-2 imagery identified more areas with moderate fire severity and fewer unburnt areas compared to Landsat 8–9 imagery (Table 2, Fig. 4). Sentinel 2 captured 40.49 % of areas as unburnt for Morgan Hollow compared to 67.81 % as unburnt captured by Landsat 8–9 and identified more pixels as low and moderate-low fire severity class (58.36 % and 1.45 %, respectively) compared to Landsat 8–9 (32.04 % for low fire severity and 0.16 % for moderate-low fire severity). For the Loper Hollow East, Sentinel 2 imagery captured fewer pixels as unburnt and low fire severity (6.86 % and 76.93 % respectively) compared to Landsat 8–9 (8.77 % and 89.95 % respectively) and captured more pixels with moderate-low fire severity class (16.20 %) compared to Landsat 8–9 (1.28 %). Only Sentinel 2 captured moderate-high fire severity class in Loper Hollo East with a value of 0.01 % account for the total areas.

For the fall burn at Stony Creek, Sentinel-2 captured a higher percentage of unburnt areas with a value of 10.78 % compared to Landsat 8 with unburnt areas of 0.10 %. The largest difference between the two sensors is found in the low and moderate-low severity class, with Sentinel-2 detecting 74.31 % of the area as low severity, compared to 10.68 % by Landsat 8, and Landsat 8 captured a larger portion in the moderate-low class (85.16 %) compared to Sentinel-2 (14.80 %). Landsat 8 detected more moderate-high severity areas with a value of 4.06 % compared to Sentinel-2 (0.11 %).

3.4. Season and spatial variation of dNBR

Fire severity maps in Fig. 4 displayed seasonal and spatial patterns of fire severity. The results showed that fall burns have significantly higher dNBR values compared to spring burns for both Sentinel-2 and Landsat 8–9 sensors (Fig. 5). For the fall burn, both Sentinel-2 and Landsat 8–9 derived dNBR displayed that north-facing aspects have the lowest value and are significantly lower than south-facing aspects. For the spring burns, south-facing and western-facing aspects displayed significantly higher dNBR values compared to north-facing and eastern-facing aspects for Sentinel 2; south-facing and western-facing aspects showed significantly higher dNBR values compared to eastern-facing aspects for Landsat 8–9 sensors.

4. Discussion

4.1. The relationship between dNBR and fire temperature

This study demonstrates the empirical relationship between satellite-derived dNBR and ground measurements of fire temperature based on 209 plots in mixed-oak forests of North-Central Appalachia. Both Landsat 8–9 and Sentinel-2 derived dNBR displayed significant positive relationships with fire temperature for the spring burns. Previous studies have verified the accuracy of dNBR as an index of fire severity by comparing satellite-derived dNBR with field measurements (Delcourt et al., 2021; Giddey et al., 2022), and proved that dNBR provides significantly accurate results for the assessment of total burn area and measurement of fire severity (Escuin et al., 2008; Öncü and Çorumluoğlu, 2023). Thus, the relationship between dNBR and fire temperature found in this study combined with the accuracy of dNBR for fire severity measurement indicates the possibility of using the Satellite-derived fire severity index (dNBR) to retrospectively infer fire temperature and provide a spatial continuous fire temperature and severity map, in a way that cannot be completely done with fieldwork alone.

When comparing the relationship between fire temperature and dNBR over Landsat 8–9 and Sentinel-2 sensors, the dNBR derived by Sentinel-2 displayed a better fit to fire temperature with a higher R^2 compared to Landsat 8–9. Part of the reason might be the higher spatial resolutions of Sentinel 2 images, which can capture finer scale spatial variability in dNBR with a resolution of 10 m compared to the 30 m resolution of Landsat 8–9. The other reason might be the date of image acquisition. The Sentinel-2 satellite has a shorter revisit time of 5 days, and the downloaded Sentinel-2 images date was closer to the actual burn date compared to the revisit time of 8 days for Landsat 8–9 images. The image acquisition time is shown in Table 1. Sentinel-2 images dated closer to the actual burn date mean that they are more sensitive to capturing the changes caused by the burn and perform better in minimizing the effects of plant regrowth or leaf drop (Konkathi and Shetty, 2021; Munyati, 2017). Additionally, neither Landsat 8–9 nor Sentinel-2 derived dNBR displayed significant correlations with fire temperature for fall burns.

4.2. Comparison between Sentinel 2 and Landsat 8–9 sensors

The results indicated that Sentinel 2 and Landsat 8–9 performed differently in capturing fire severity over spring and fall burns. For the spring burns, Sentinel 2 can capture higher dNBR values compared to Landsat 8–9 imagery; however, for the fall burn, Landsat 8–9 imagery captured higher dNBR values than Sentinel 2.

The results of spring burns are consistent with previous studies that even though Sentinel 2 and Landsat 8–9 sensors performed similarly in the detection of fire extent, Sentinel 2 tends to map burnt areas as one higher severity class compared to Landsat 8–9 sensor, and Sentinel 2 produces smaller proportions of low severity and larger proportions of high severity (Konkathi and Shetty, 2021; White and Gibson, 2022). The inconsistency in fire severity classification between the two sensors is expected, due to the spectral similarity between adjacent classes, where only one severity class differs, and the effects of sub-pixel mixing resulting from the varying resolutions of the sensors (White and Gibson, 2022). Conversely, Howe et al., (2022) found a higher fire severity estimated by Landsat 8 compared to Sentinel-2, which is consistent with our fall burn results. Howe et al., (2022) mentioned that the difference in fire severity classification is primarily driven by the difference in resolution, and this often occurs at the edge of each fire severity patch, indicating that mapping burn severity at higher resolution could help delineate fire severity patches (Miller et al., 2009).

Additionally, the seasonal effects on fire severity have been detected by Verbyla et al., (2008), which demonstrates a decrease in NBR with decreasing solar elevation and explains that seasonal changes in NBR may be influenced by a combination of changes in leaf, vegetation senescence, and solar elevation. Thus, pre-fire and post-fire image acquisition on the same day or close to the actual burn day is highly recommended to minimize the noise of leaf drop and solar elevation effects on dNBR values (Chen et al., 2020). In this study, the Landsat 8–9 image acquisition has a broader time range compared to Sentinel 2 (shown in Table 2). Plus, the Landsat 8–9 images were acquired in late fall during leaf drop, which may introduce greater uncertainty in the derived dNBR, as it captures changes caused by both leaf drop and fire.

The Landsat image acquisition time may also explain the lack of significant relationships between fire temperature and dNBR. Spectral indices tend to correlate better with surface variables due to the shielding effect of the inadequacies of sensors to detect under surface conditions (Tanase et al., 2011). Therefore, the leaf drop in post-fire imagery may influence dNBR. Additionally, tree canopy cover is sparse in late fall owing to marcescence, the withering of the leaves on a plant without abscission and leaf fall during autumn and winter, especially for oak and American beech (Sánchez De Dios et al., 2009), which are abundant in our study area. The sparse and low canopy cover can influence satellite reflectance and cause higher noise levels, making it difficult to estimate ground changes caused by fire.

Overall, these results suggest that combining Sentinel-2 and Landsat 8–9 datasets could provide a more comprehensive understanding of fire severity patterns, and image-acquiring time can, to some extent,

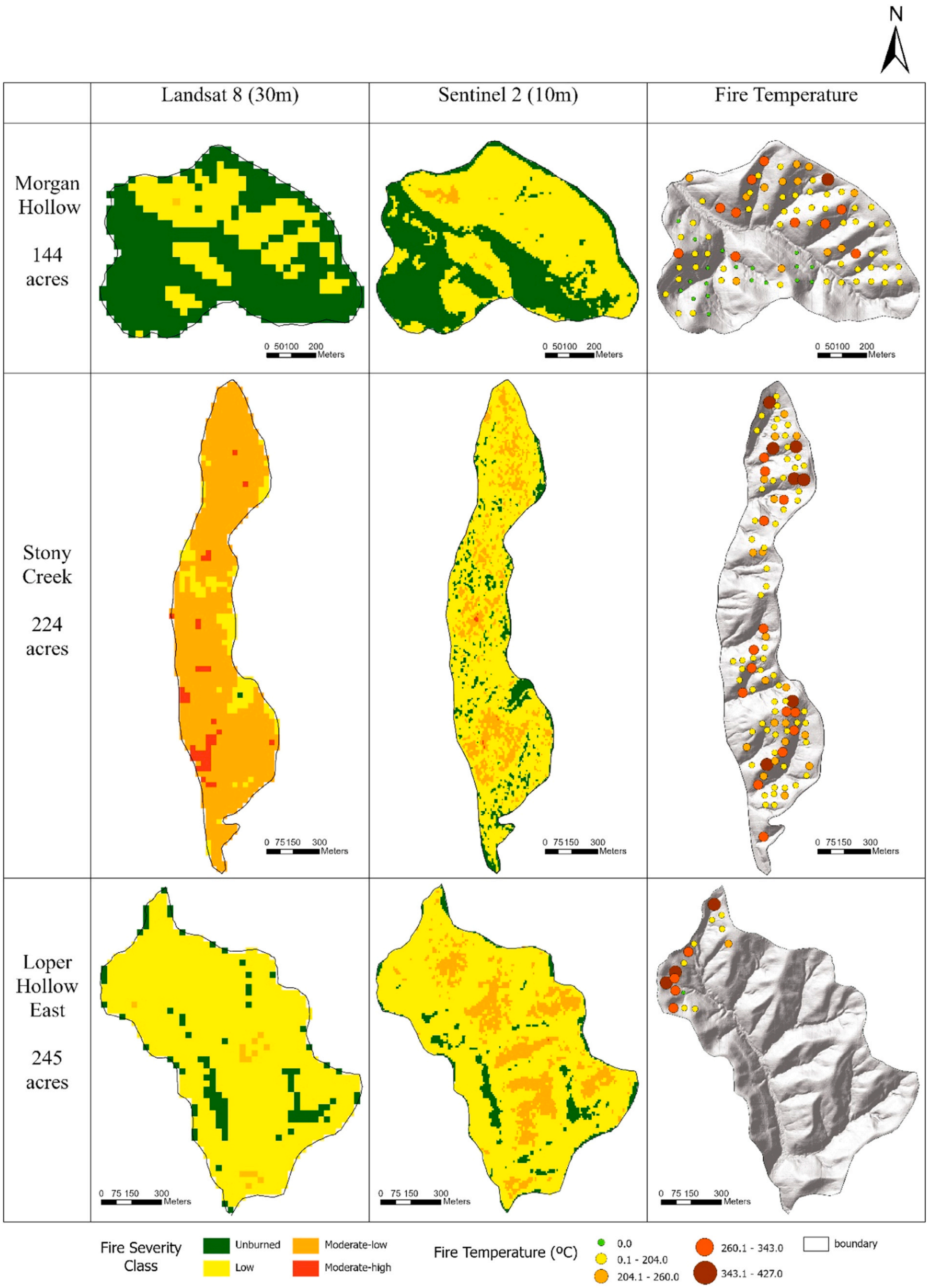

Fig. 4. Differenced Normalized Burn Ratio (dNBR) mapped with both Sentinel 2 and Landsat 8 imagery and fire temperature maps of the three study sites.

Table 2
Summary of fire severity classification and the percentage of each fire severity class count for the total area in each study site based on the dNBR values calculated from Sentinel-2 and Landsat 8–9 imagery. The fire severity classification was proposed by United States Geological Survey (USGS).

Site	Burn Season	Severity class	dNBR range (scaled by 10^3)	dNBR range (not scaled)	Percentage	
					Landsat 8	sentinel-2
MH	Spring	Unburnt	−100 to + 99	−0.100 to + 0.099	67.81	40.49
		low	+ 100 to + 269	+ 0.100 to + 0.269	32.04	58.36
		Moderate-low	+ 270 to + 439	+ 0.270 to + 0.439	0.16	1.45
		Moderate-high	+ 440 to + 659	+ 0.440 to + 0.659	0	0
SK	Fall	unburnt	−100 to + 99	−0.100 to + 0.099	0.10	10.78
		low	+ 100 to + 269	+ 0.100 to + 0.269	10.68	74.31
		Moderate-low	+ 270 to + 439	+ 0.270 to + 0.439	85.16	14.80
		Moderate-high	+ 440 to + 659	+ 0.440 to + 0.659	4.06	0.11
LE	Spring	unburnt	−100 to + 99	−0.100 to + 0.099	8.77	6.86
		low	+ 100 to + 269	+ 0.100 to + 0.269	89.95	76.93
		Moderate-low	+ 270 to + 439	+ 0.270 to + 0.439	1.28	16.20
		Moderate-high	+ 440 to + 659	+ 0.440 to + 0.659	0	0.01

influence overall dNBR values.

4.3. Seasonal and spatial patterns of dNBR

Seasonal and spatial patterns of dNBR were examined in this study, with the fall burn having higher dNBR values compared to spring burns for both Sentinel 2 and Landsat 8–9 sensors, and south-facing aspects usually having higher dNBR values compared to north-facing aspects. Previous research in the North-Central Appalachia region demonstrated that fall burns have significantly higher fire temperatures compared to spring burns, and south-facing aspects displayed higher fire temperatures compared to north-facing aspects for both spring and fall burns (Schwemlein and Williams, 2007). Based on the statistically significant correlation between fire temperature and dNBR in this research, the spatial and seasonal patterns of dNBR are consistent with the fire temperature patterns. Additionally, Dong and Williams, (2024) revealed that fuel bed composition changed across aspects and slope position, which is a primary factor influencing the environment where fire occurs. Specifically, southern aspects have the highest oak component in the fuel loading, while north-facing aspects usually have a lower proportion of oak fuel (Dong and Williams, 2024). Different fuel compositions combined with different flammability of species that oak fuels tend to have higher flammability and produce a hotter fire temperature than other species (Dong and Williams, 2023; McDaniel et al., 2021) can reveal that different aspects are expected to have different fire risks and fire severity, which was demonstrated in this study.

5. Conclusion

A linkage between satellite-derived dNBR and ground measurements of fire temperature was examined in this study. Both Landsat 8–9 and Sentinel-2 derived dNBR displayed a significant positive correlation with fire temperature for the spring burns, with Sentinel-2 displaying a better fit to fire temperature compared to Landsat 8–9. When using dNBR to assess fire severity, Sentinel 2 can capture higher dNBR values compared to Landsat 8–9 imagery in the spring; however, Landsat 8–9 imagery captured higher dNBR in the fall burn. This comparison of spring and fall burns highlights that satellite performance might vary depending on the burn season. Additionally, the seasonal and spatial patterns of fire severity were detected with fall burns having higher fire severity compared to spring burns and south-facing aspects usually

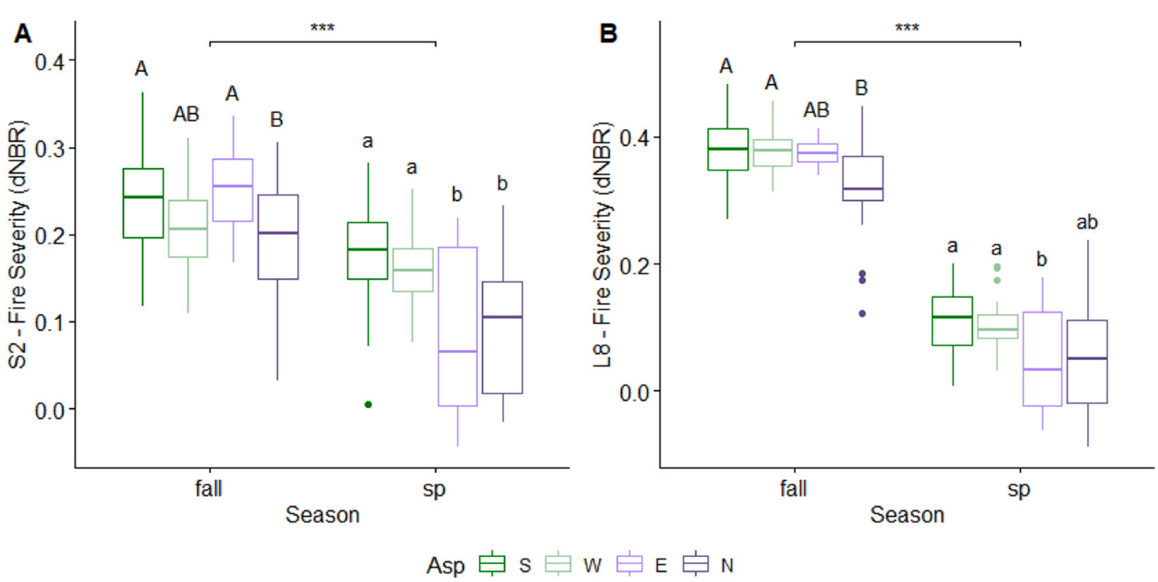

Fig. 5. The relationship between dNBR across seasons and aspects (S, W, E, N). Specifically, (A) Sentinel 2 derived dNBR and (B) Landsat 8–9 derived dNBR across spring and fall seasons over different aspects. Figures with the same letters in each group are not different between aspects (post hoc Tukey–Kramer test, p = 0.05). *** Significant at the 0.001 level.

having higher dNBR values compared to north-facing aspects.

In this study, the limitations remain in the fire temperature measurement. The fire temperatures were measured by pyrometer and calibrated by thermocouples, there might be some errors in the fire temperature measurements that can affect the relationship between fire temperature and satellite-derived dNBR as pyrometers can only provide an estimated range of fire temperature. Even though the calibrated fire temperature displayed a strong positive correlation with satellite-derived dNBR for both sensors, a more accurate measurement of fire temperature is needed. Overall, these findings can provide a potential method to map spatial continuous fire temperature maps by retrospectively inferring fire temperature using satellite-based dNBR, filling the gaps that fieldwork can only measure discrete fire temperature, providing a cost-efficient and more accessible method to map fire temperature compared to the use of LWIR imagery or UAVs.

CRediT authorship contribution statement

Dong Ziyu: Writing – original draft, Methodology, Formal analysis, Data curation, Conceptualization. **Williams Roger A.:** Writing – review & editing, Supervision, Resources, Project administration, Funding acquisition.

Declaration of Competing Interest

The authors declare the following financial interests/personal relationships which may be considered as potential competing interests: Roger Williams reports financial support was provided by National Science Foundation. Roger Williams reports financial support was provided by McIntire-Stennis. If there are other authors, they declare that they have no known competing financial interests or personal relationships that could have appeared to influence the work reported in this paper.

Acknowledgments

Funding for this study was provided by the National Science Foundation National Robotics Initiative, award number 2132798, and McIntire-Stennis project OHO00058-MS.

Data Availability

Data will be made available on request.

References

Achour, H., Toujani, A., Trabelsi, H., Jaouadi, W., 2022. Evaluation and comparison of Sentinel-2 MSI, Landsat 8 OLI, and EFFIS data for forest fires mapping. Illustrations from the summer 2017 fires in Tunisia. Geocarto Int. 37 (24), 7021–7040. https://doi.org/10.1080/10106049.2021.1980118.

Agbeshie, A.A., Abugre, S., Atta-Darkwa, T., Awuah, R., 2022. A review of the effects of forest fire on soil properties. J. For. Res. 33 (5), 1419–1441. https://doi.org/10.1007/s11676-022-01475-4.

Akhloufi, M.A., Couturier, A., Castro, N.A., 2021. Unmanned aerial vehicles for wildland fires: sensing, perception, cooperation and assistance. Drones 5 (1), 15. https://doi.org/10.3390/drones5010015.

Allison, R., Johnston, J., Craig, G., Jennings, S., 2016. Airborne optical and thermal remote sensing for wildfire detection and monitoring. Sensors 16 (8), 1310. https://doi.org/10.3390/s16081310.

Ambrosia, V.G., Wegener, S.S., Sullivan, D.V., Buechel, S.W., Dunagan, S.E., Brass, J.A., Stoneburner, J., Schoenung, S.M., 2003. Demonstrating UAV-acquired real-time thermal data over fires. Photogramm. Eng. Remote Sens. 69 (4), 391–402. https://doi.org/10.14358/PERS.69.4.391.

Aragon, B., Johansen, K., Parkes, S., Malbeteau, Y., Al-Mashharawi, S., Al-Amoudi, T., Andrade, C.F., Turner, D., Lucieer, A., McCabe, M.F., 2020. A calibration procedure for field and UAV-based uncooled thermal infrared instruments. Sensors 20 (11), 3316. https://doi.org/10.3390/s20113316.

Bataineh, M., Portner, B., Pelkki, M., Ficklin, R., 2022. Prescribed fire first-order effects on oak and maple reproduction in frequently burned upland oak–hickory forests of the Arkansas ozarks. Forests 13 (11), 1865. https://doi.org/10.3390/f13111865.

Boerner, R.E.J., Morris, S.J., Sutherland, E.K., Hutchinson, T.F., 2000. Spatial variability in soil nitrogen dynamics after prescribed burning in Ohio mixed-oak forests. Landsc. Ecol. 15 (5), 425–439. https://doi.org/10.1023/A:1008179702536.

Cansler, C.A., McKenzie, D., 2014. Climate, fire size, and biophysical setting control fire severity and spatial pattern in the northern Cascade Range, USA. Ecol. Appl. 24 (5), 1037–1056. https://doi.org/10.1890/13-1077.1.

Chen, D., Loboda, T.V., Hall, J.V., 2020. A systematic evaluation of influence of image selection process on remote sensing-based burn severity indices in North American boreal forest and tundra ecosystems. ISPRS J. Photogramm. Remote Sens. 159, 63–77. https://doi.org/10.1016/j.isprsjprs.2019.11.011.

Collins, L., Bennett, A.F., Leonard, S.W.J., Penman, T.D., 2019. Wildfire refugia in forests: Severe fire weather and drought mute the influence of topography and fuel age. Glob. Change Biol. 25 (11), 3829–3843. https://doi.org/10.1111/gcb.14735.

Delcourt, C.J.F., Combee, A., Izbicki, B., Mack, M.C., Maximov, T., Petrov, R., Rogers, B. M., Scholten, R.C., Shestakova, T.A., Van Wees, D., Veraverbeke, S., 2021. Evaluating the Differenced Normalized Burn Ratio for Assessing Fire Severity Using Sentinel-2 Imagery in Northeast Siberian Larch Forests. Remote Sens. 13 (12), 2311. https://doi.org/10.3390/rs13122311.

Dennison, P., Charoensiri, K., Roberts, D., Peterson, S., Green, R., 2006. Wildfire temperature and land cover modeling using hyperspectral data. Remote Sens. Environ. 100 (2), 212–222. https://doi.org/10.1016/j.rse.2005.10.007.

Dickinson, M.B., Hudak, A.T., Zajkowski, T., Loudermilk, E.L., Schroeder, W., Ellison, L., Kremens, R.L., Holley, W., Martinez, O., Paxton, A., Bright, B.C., O'Brien, J.J., Hornsby, B., Ichoku, C., Faulring, J., Gerace, A., Peterson, D., Mauceri, J., 2016. Measuring radiant emissions from entire prescribed fires with ground, airborne and satellite sensors – RxCADRE 2012. Int. J. Wildland Fire 25 (1), 48. https://doi.org/10.1071/WF15090.

Dong, Z., Williams, R.A., 2023. Effects of Wildland Fuel Composition on Fire Intensity. Fire 6 (8), 312. https://doi.org/10.3390/fire6080312.

Dong, Z., Williams, R.A., 2024. Characterization of Wildland Fuels Based on Topography and Forest Attributes in North-Central Appalachia. Fire 7 (4), 145. https://doi.org/10.3390/fire7040145.

Escuin, S., Navarro, R., Fernández, P., 2008. Fire severity assessment by using NBR (Normalized Burn Ratio) and NDVI (Normalized Difference Vegetation Index) derived from LANDSAT TM/ETM images. Int. J. Remote Sens. 29 (4), 1053–1073. https://doi.org/10.1080/01431160701281072.

Freeborn, P.H., Wooster, M.J., Hao, W.M., Ryan, C.A., Nordgren, B.L., Baker, S.P., Ichoku, C., 2008. Relationships between energy release, fuel mass loss, and trace gas and aerosol emissions during laboratory biomass fires. J. Geophys. Res.: Atmospheres 113 (D1), 2007JD008679. https://doi.org/10.1029/2007JD008679.

Gale, M.G., Cary, G.J., Van Dijk, A.I.J.M., Yebra, M., 2021. Forest fire fuel through the lens of remote sensing: Review of approaches, challenges and future directions in the remote sensing of biotic determinants of fire behaviour. Remote Sens. Environ. 255, 112282. https://doi.org/10.1016/j.rse.2020.112282.

Giddey, B.L., Baard, J.A., Kraaij, T., 2022. Verification of the differenced Normalised Burn Ratio (dNBR) as an index of fire severity in Afrotemperate Forest. South Afr. J. Bot. 146, 348–353. https://doi.org/10.1016/j.sajb.2021.11.005.

Hammill, K.A., Bradstock, R.A., 2006. Remote sensing of fire severity in the Blue Mountains: Influence of vegetation type and inferring fire intensity. Int. J. Wildland Fire 15 (2), 213. https://doi.org/10.1071/WF05051.

Howe, A.A., Parks, S.A., Harvey, B.J., Saberi, S.J., Lutz, J.A., Yocom, L.L., 2022. Comparing Sentinel-2 and Landsat 8 for Burn Severity Mapping in Western North America. Remote Sens. 14 (20), 5249. https://doi.org/10.3390/rs14205249.

Hudak, A.T., Dickinson, M.B., Bright, B.C., Kremens, R.L., Loudermilk, E.L., O'Brien, J.J., Hornsby, B.S., Ottmar, R.D., 2016. Measurements relating fire radiative energy density and surface fuel consumption – RxCADRE 2011 and 2012. Int. J. Wildland Fire 25 (1), 25. https://doi.org/10.1071/WF14159.

Iverson, L.R., Yaussy, D.A., Rebbeck, J., Hutchinson, T.F., Long, R.P., Prasad, A.M., 2004. A comparison of thermocouples and temperature paints to monitor spatial and temporal characteristics of landscape-scale prescribed fires. Int. J. Wildland Fire 13 (3), 311. https://doi.org/10.1071/WF03063.

Kanand, T., Kemper, G., König, R., Kemper, H., 2020. WILDFIRE DETECTION AND DISASTER MONITORING SYSTEM USING UAS AND SENSOR FUSION TECHNOLOGIES. Int. Arch. Photogramm., Remote Sens. Spat. Inf. Sci. XLIII-B3-2020, 1671–1675. https://doi.org/10.5194/isprs-archives-XLIII-B3-2020-1671-2020.

Kaufman, Y.J., Kleidman, R.G., King, M.D., 1998. SCAR-B fires in the tropics: Properties and remote sensing from EOS-MODIS. J. Geophys. Res.: Atmospheres 103 (D24), 31955–31968. https://doi.org/10.1029/98JD02460.

Keeley, J.E., 2009. Fire intensity, fire severity and burn severity: A brief review and suggested usage. Int. J. Wildland Fire 18 (1), 116. https://doi.org/10.1071/WF07049.

Konkathi, P., Shetty, A., 2021. Inter comparison of post-fire burn severity indices of Landsat-8 and Sentinel-2 imagery using Google Earth Engine. Earth Sci. Inform. 14 (2), 645–653. https://doi.org/10.1007/s12145-020-00566-2.

Kremens, R.L., Dickinson, M.B., Bova, A.S., 2012. Radiant flux density, energy density and fuel consumption in mixed-oak forest surface fires. Int. J. Wildland Fire 21 (6), 722. https://doi.org/10.1071/WF10143.

McDaniel, J.K., Alexander, H.D., Siegert, C.M., Lashley, M.A., 2021. Shifting tree species composition of upland oak forests alters leaf litter structure, moisture, and flammability. For. Ecol. Manag. 482, 118860. https://doi.org/10.1016/j.foreco.2020.118860.

Miller, J.D., Knapp, E.E., Key, C.H., Skinner, C.N., Isbell, C.J., Creasy, R.M., Sherlock, J. W., 2009. Calibration and validation of the relative differenced Normalized Burn Ratio (RdNBR) to three measures of fire severity in the Sierra Nevada and Klamath

Mountains, California, USA. Remote Sens. Environ. 113 (3), 645–656. https://doi.org/10.1016/j.rse.2008.11.009.

Molina, J.R., Ortega, M., Rodríguez y Silva, F., 2022. Fire ignition patterns to manage prescribed fire behavior: Application to Mediterranean pine forests. J. Environ. Manag. 302, 114052. https://doi.org/10.1016/j.jenvman.2021.114052.

Mueller, E.V., Skowronski, N., Thomas, J.C., Clark, K., Gallagher, M.R., Hadden, R., Mell, W., Simeoni, A., 2018. Local measurements of wildland fire dynamics in a field-scale experiment. Combust. Flame 194, 452–463. https://doi.org/10.1016/j.combustflame.2018.05.028.

Munyati, C., 2017. The potential for integrating Sentinel 2 MSI with SPOT 5 HRG and Landsat 8 OLI imagery for monitoring semi-arid savannah woody cover. Int. J. Remote Sens. 38 (17), 4888–4913. https://doi.org/10.1080/01431161.2017.1331057.

Öncü, G., & Çorumluoğlu, Ö. (2023). Determination of Spatial Distribution of Damage Intensity of Tınazlı-Izmir Forest Fire Using Remote Sensing Indexing Techniques.

Parks, S., Dillon, G., Miller, C., 2014. A new metric for quantifying burn severity: the relativized burn ratio. Remote Sens. 6 (3), 1827–1844. https://doi.org/10.3390/rs6031827.

Perry, D.A., Hessburg, P.F., Skinner, C.N., Spies, T.A., Stephens, S.L., Taylor, A.H., Franklin, J.F., McComb, B., Riegel, G., 2011. The ecology of mixed severity fire regimes in Washington, Oregon, and Northern California. For. Ecol. Manag. 262 (5), 703–717. https://doi.org/10.1016/j.foreco.2011.05.004.

Quintano, C., Fernández-Manso, A., Fernández-Manso, O., 2018. Combination of Landsat and Sentinel-2 MSI data for initial assessing of burn severity. Int. J. Appl. Earth Obs. Geoinf. 64, 221–225. https://doi.org/10.1016/j.jag.2017.09.014.

Roy, D.P., Boschetti, L., Trigg, S.N., 2006. Remote sensing of fire severity: Assessing the performance of the normalized burn ratio. IEEE Geosci. REMOTE Sens. Lett. 3 (1).

Sánchez De Dios, R., Benito-Garzón, M., Sainz-Ollero, H., 2009. Present and future extension of the Iberian submediterranean territories as determined from the distribution of marcescent oaks. Plant Ecol. 204 (2), 189–205. https://doi.org/10.1007/s11258-009-9584-5.

Schwemlein, D.J., Williams, R.A., 2007. Effects of Landscape Position and Season of Burn on Fire Temperature in Southern Ohio's Mixed Oak Forests, 8.

Silvani, X., Morandini, F., 2009. Fire spread experiments in the field: Temperature and heat fluxes measurements. Fire Saf. J. 44 (2), 279–285. https://doi.org/10.1016/j.firesaf.2008.06.004.

Tanase, M., De La Riva, J., Pérez-Cabello, F., 2011. Estimating burn severity at the regional level using optically based indices. Can. J. For. Res. 41 (4), 863–872. https://doi.org/10.1139/x11-011.

Verbyla, D.L., Kasischke, E.S., Hoy, E.E., 2008. Seasonal and topographic effects on estimating fire severity from Landsat TM/ETM+ data. Int. J. Wildland Fire 17 (4), 527. https://doi.org/10.1071/WF08038.

Wardihani, E.D., Ramdhani, M., Suharjono, A., Setyawan, T.A., Hidayat, S.S., Widodo, S., Triyono, E., Saifullah, F., 2018. REAL-TIME FOREST FIRE MONITORING SYSTEM USING UNMANNED. Aer. Veh. 13.

White, L.A., Gibson, R.K., 2022. Comparing Fire Extent and Severity Mapping between Sentinel 2 and Landsat 8 Satellite Sensors. Remote Sens. 14 (7), 1661. https://doi.org/10.3390/rs14071661.

Wooster, M.J., Roberts, G., Perry, G.L.W., Kaufman, Y.J., 2005. Retrieval of biomass combustion rates and totals from fire radiative power observations: FRP derivation and calibration relationships between biomass consumption and fire radiative energy release. J. Geophys. Res.: Atmospheres 110 (D24), 2005JD006318. https://doi.org/10.1029/2005JD006318.